Tailoring the isothermal crystallization kinetics of isodimorphic poly (butylene succinate-*ran*-butylene azelate) random copolymers by changing composition

Idoia Arandia [a], Nerea Zaldua [a], Jon Maiz [a], Ricardo A. Pérez-Camargo [a], Agurtzane Mugica [a], Manuela Zubitur [b], Rosica Mincheva [c], Philippe Dubois [c], Alejandro J. Müller [a,d,*]

[a] POLYMAT and Polymer Science and Technology Department, Faculty of Chemistry, University of the Basque Country UPV/EHU, Paseo Manuel de Lardizabal 3, 20018, Donostia-San Sebastián, Spain
[b] Chemical and Environmental Engineering Department, Polytechnic School, University of the Basque Country UPV/EHU, 2008, Donostia-San Sebastián, Spain
[c] Laboratory of Polymeric and Composite Materials, Center of Innovation and Research in Materials and Polymers (CIRMAP),University of Mons (UMONS), Place du Parc 20, 7000, Mons, Belgium
[d] IKERBASQUE, Basque Foundation for Science, Bilbao, Spain

ARTICLE INFO

ABSTRACT

A detailed isothermal crystallization study of biobased and biodegradable isodimorphic poly (butylene succinate-*ran*-butylene azelate) random copolyesters (PBS-*ran*-PBAz) with a wide composition range has been carried out to determine nucleation kinetics, spherulitic growth rates and overall crystallization kinetics. Differential Scanning Calorimetry (DSC) and Polarized Light Optical Microscopy (PLOM) analysis show that for the PBS-rich phase, the incorporation of BAz comonomer leads to a significant increase in nucleation density and a decrease in spherulitic growth. On the contrary, for the PBAz-rich phase, an antinucleating effect of the incorporation of BS comonomer has been observed. Both effects agree with the thermodynamic analysis of the equilibrium melting point depression as a function of composition, which predicts that only a small amount of BAz comonomer is included within the PBS-rich crystals and a larger amount of comonomer is included in PBAz-rich crystals. In addition, the enthalpy of melting of 100% crystalline PBS and PBAz were determined by a different practical approach: extrapolating real time synchrotron Wide Angle X-ray Scattering (WAXS) isothermal crystallization data and isothermal DSC data.

1. Introduction

Biodegradable and biobased polymers are considered potential substitutes of traditional non-biodegradable polymeric materials. Among these, aliphatic polyesters, such as poly (lactic acid) (PLA), poly (ε-caprolactone) (PCL), poly (butylene succinate) (PBS), and poly (butylene azelate) (PBAz), are the most promising materials. They are obtained from renewable sources and have attracted increasing interest in a large range of applications in textile and agricultural industries, packaging, and biomedical devices because of their biodegradability and biocompatibility [1–3]. Unfortunately, their applications are limited in some cases by inadequate mechanical properties and/or by a slow biodegradation rate caused by their high degree of crystallinity.

Therefore, with the aim of adapting these properties, the synthesis of random copolyesters, with biobased comonomers, has been accomplished to obtain versatile random copolymers [4–9].

The properties of crystallizable random copolymers constituted by two potentially semi-crystalline parent components have been recently reviewed [10]. Depending on their miscibility and ability to share crystal lattices, three different cases have been reported [11]. The most commonly reported case is the total exclusion of the comonomer that constitutes the minor component from the crystalline regions of the major component. In this case, the copolymers are unable to crystallize in a wide composition range. Only compositions containing typically 10 mol % or less of the second comonomer are able to crystallize. This case usually arises when comonomers chemical structures are very

---

different from one another.

On the other hand, only when the chemical structures of both co-monomers are similar, two cases of co-crystallization may occur: isomorphism or isodimorphism [10,12]. In isomorphic copolymers, total comonomer inclusion inside the crystal unit cell occurs, therefore only one crystalline phase containing both comonomer units is formed and only one crystalline structure is obtained for all compositions [9,13–15].

In isodimorphic copolymers, the random copolymers also crystallize in the whole composition range, but with two crystal structures that resemble those of the parent homopolymers depending on composition, and at least one of the two crystalline phases includes some comonomeric units of the minor component in their crystal lattice. Isodimorphic copolymers also show a pseudo-eutectic behaviour when their thermal transitions, such as melting and crystallization temperatures, are plotted as a function of composition, and the eutectic point is located at the composition at which a change in crystal structure occurs. On each side of the pseudo-eutectic point, only the crystalline phase of the major component is formed, which may contain a limited amount of the minor comonomer chains included in the crystal lattice. It is usually observed that with the addition of minor comonomer units, the crystallization and melting temperatures of the copolymers decreases [16]. Additionally, we have previously demonstrated that at the pseudo-eutectic point, two crystalline phases can form and co-exist within double crystalline spherulites [10].

In previous works, we have studied the morphology and non-isothermal crystallization of poly (butylene succinate-*ran*-butylene azelate) (PBSAz) copolyesters previously synthesized by Mincheva et al. and presented in ref. 17. Both main components of these interesting copolymers are biodegradable and their monomers are derived from biomass. Poly (butylene succinate) (PBS) is well known for its good mechanical properties, easy processability and relatively low production cost [18–20]. The copolymers are isodimorphic as poly (butylene azelate) (PBAz) has the same functional groups as PBS and they differentiate only in the length of the corresponding dicarboxylic acid [4]. Wide Angle X-Ray Scattering (WAXS) measurements showed that due to a partial comonomer inclusion, small variations in the crystalline unit cell dimensions of the dominant crystalline phase were found. Also, Differential Scanning Calorimetry (DSC) measurements showed that the thermal transitions temperatures (i.e., T_c and T_m) went through a pseudo-eutectic point when plotted as a function of composition. Furthermore, thermal fractionation by Successive Self-nucleation and Annealing (SSA), which promotes segregation of molecular defects that interrupt crystallizable sequences, was performed and signs of co-crystallization were still detected [21]. The study of the dielectric relaxation of PBSAz copolymers was also performed [22]. In this previous work, the dynamics of the comonomers remaining in the amorphous phase were analyzed, and it was possible to quantify the comonomer fraction participating in the crystalline and amorphous phases.

Puiggali et al. [23] previously studied the crystallization of similar PBSAz copolymers. The possible co-crystallization behavior was analyzed by comparing the experimental estimations of the equilibrium melting points, with exclusion-inclusion models available in the literature [10]. They concluded that their copolymers behavior could be explained by total comonomer exclusion, in spite of the fact that their copolymers were able to crystallize in the entire composition range examined.

In the present work, we perform for the first time, detailed isothermal studies of the nucleation kinetics, spherulitic growth rates and overall crystallization kinetics of PBSAz copolymers in a wide composition range to demonstrate the dramatic influence of composition on crystallization kinetics. By measuring nucleation, growth and overall crystallization kinetics, we are able to ascertain which factors determine the final solidification kinetics of the copolymers and assess the influence of composition. In addition, we determine the enthalpy of melting of 100% crystalline PBS and PBAz by a different and practical approach: extrapolating real time synchrotron WAXS isothermal crystallization data and isothermal DSC data. Finally, by applying thermodynamic models to the equilibrium melting point data as a function of composition, we are able to calculate the amount of comonomer inclusion within each crystalline phase and correlate these results with the trends in crystallization rate with composition.

2. Experimental section

2.1. Materials

The PBSAz copolymers were synthesized by a two-stage melt polycondensation reaction. This consisted in an esterification at atmospheric pressure of diacid (co)monomer(s) and a diol, and polycondensation of the obtained oligoesters to (co)polymers at reduced pressure. Reactions were performed in a expressly designed and adapted Inox Autoclave reactor (Autoclave-France, France). Succinic acid (SuA) and dimethyl azelate (DMAz) were copolymerized at [COOH]: [COOCH$_3$] = 1.0:0, 0.8:0.2, 0.6:0.4, 0.5:0.5, 0.4:0.6, 0.2:0.8, and 0:1.0 M ratios in the presence of 1,4-butanediol (BDO). The details of the synthesis have been previously reported [17]. Samples are denoted in an abbreviated form, e.g., BS$_{xx}$BAz$_{yy}$, indicating the molar ratio of each component as subscripts (xx and yy) and are specified in Table 1.

2.2. Polarized Light Optical Microscopy (PLOM)

An Olympus BX51 polarized light optical microscope was used with a Linkam THMS600 hot stage for accurate temperature control. The appearance of nuclei was recorded as a function of time during isothermal crystallization from the melt. Samples were first melted, at a temperature 30 °C higher than the melting point of the sample determined by DSC, to erase their thermal history for 3 min. Then they were quickly cooled down to the chosen T_c value.

Spherulite growth rate experiments were also performed by recording their growth by PLOM (Olympus BX51), incorporating a λ plate in between the polarizers at 45° to facilitate observation and determine the sign of the birefringence. The dimensions of the spherulites were periodically registered with an Olympus SC50 digital camera. The samples were placed in between of a glass slide and a glass coverslip. The conditions used for the isothermal experiments were very similar to the DSC ones, where samples were first heated to a temperature of 30 °C above their DSC melting peak to erase their thermal history and then crystallized from the melt to a selected isothermal crystallization temperature (T_c) at 60 °C/min employing the Linkam THMS600 hot stage.

2.3. Isothermal crystallization kinetics

Isothermal crystallization experiments were performed with a

Table 1
Molar composition determined by ^{1}H NMR, number-average molecular weight determined by SEC and thermal transitions determined by DSC (at 10 °C/min) of the materials employed in this work.

	Code	Composition (PBS/PBAz), mol ^{1}H NMR	Mn (g/mol) SEC	Đ	DSC Data [4]		
					T_g (°C)	T_{m1} (°C)	T_{m2} (°C)
1	BS	1/0	25.300	2.36	−36	115	–
2	BS$_{82}$BAz$_{18}$	0.82/0.18	22.300	1.76	−50	98	–
3	BS$_{61}$BAz$_{39}$	0.61/0.39	31.300	5.16	−56	72	–
4	BS$_{58}$BAz$_{42}$	0.58/0.42	36.500	3.44	−57	60	–
5	BS$_{45}$BAz$_{55}$	0.45/0.55	38.300	3.24	−61	46	26
6	BS$_{25}$BAz$_{75}$	0.25/0.75	39.600	3.45	−62	–	34
7	BAz	0/1	42.500	2.42	−63	–	41

Estimation of errors is based on the repetition of DSC experiments; calibration and baseline drifts indicate that transition temperatures are valid within 0.5 °C (except for T_g measurements which are within 1 °C).

PerkinElmer Pyris 1 differential scanning calorimetry (DSC), which contains a refrigerated cooling system (Intracooler 2P). It was calibrated with indium and tin standards. For the measurements, which were made under a nitrogen atmosphere flow, $\cong 5$ mg, samples were sealed in aluminum pans and the procedure followed was that recommended by Lorenzo et al. [24]. Overall isothermal crystallization experiments were performed by directly quenching the samples from the melt at 60 °C/min. Before starting with the isothermal procedure, the minimum isothermal crystallization temperature was first determined. This was done by heating the sample directly from the chosen T_c value, after being quenched from the melt (at 60 °C/min). The lowest temperature which did not show any melting enthalpy during immediate subsequent heating was the minimum isothermal crystallization temperature employed [24].

The samples were heated to 30 °C above their melting temperature for 3 min in order to erase the previous thermal history, and then cooled at a rate of 60 °C/min (at which the calorimeter can control the cooling rate) to the chosen isothermal crystallization temperature T_c. At these chosen T_c values, the samples were left to crystallize until saturation, and finally they were heated up from T_c to 30 °C above their peak melting temperature at 20 °C/min.

The complimentary origin plug-in developed by Lorenzo et al. [24] was employed to perform the fittings to the Avrami equation following the recommendations given in this paper (this plug-in is for free distribution upon request).

2.4. Simultaneous SAXS/WAXS synchrotron measurements

Simultaneous SAXS/WAXS experiments were performed at the beamline BL11-NCD, ALBA Synchrotron facility in Barcelona, Spain. A Linkam THMS600 hot stage equipped with a liquid nitrogen cooling system was used to heat and cool the samples placed inside capillaries, and while copolymers were crystallizing SAXS/WAXS patterns were periodically recorded.

In order to calculate the heat of fusion of a 100% crystalline polymer, $\Delta H^0_{m(100\%)}$, of each neat homopolymer (i.e., PBS and PBAz), the samples were heated to 30 °C above their melting point for 3 min, and then cooled to a chosen temperature at 50 °C/min. At this temperature, the samples were isothermally crystallized during 30 min while SAXS and WAXS patterns were simultaneously registered every 10 s.

The Thomson-Gibbs equation is used to calculate the equilibrium melting temperature (T^0_m) of a homopolymer if the melting point and the average value of the lamellar thickness are known for a series of isothermally crystallized samples. In the case of calculating the equilibrium melting temperature, T^0_m, all samples were isothermally crystallized at different temperatures before cooling them to room temperature at which SAXS and WAXS patterns were registered. Their melting points were separately determined by DSC.

The X-ray energy source used for WAXS/SAXS measurements was 12.4 keV ($\lambda = 1.03$ Å). Specifically, for the SAXS configuration the distance between the sample and the detector was 6495.0 mm with a tilt angle of 0° and was calibrated using silver behenate (ADSC Q315r, Poway, CA, USA, with a resolution of 3070×3070 pixels, pixel size of 102 μm^2). For the WAXS configuration, which was calibrated using chromium (III) oxide, the distance between the sample and the detector was 132.6 mm with a tilt angle of 21.2°. (Rayonix LX255-HS detector, Evanston, IL, USA, with resolution of 1920×5760 pixels, pixel size of 44 μm^2).

The intensity profiles plot the scattering intensity as a function of the scattering vector, $q = 4\pi sin\theta\lambda^{-1}$, where λ is the X-ray wavelength ($\lambda = 1.03$ Å) and 2θ is the scattering vector.

3. Results and discussion

3.1. Nucleation kinetics studied by PLOM

Examples of nucleation data obtained by PLOM are plotted in Fig. 1a–b. Both figures show the nucleation density ρ (N/mm^3) as a function of time for neat PBS and BS$_{58}$BAz$_{42}$ copolymer respectively. Data for the other samples are reported in Figure S1 of the Supplementary Information. On the other hand, due to the high nucleation density of the samples which contain only PBAz-rich crystals (i.e., BS$_{25}$BAz$_{75}$ copolymer and PBAz homopolymer), it was impossible to determine their nucleation kinetics.

The nucleation behavior observed in all samples (e.g., Fig. 1a–b) was close to instantaneous. A more detailed analysis indicates that two important parameters affect the nucleation density of PBS-rich copolymers (Fig. 1c): (a) the chosen isothermal crystallization temperature and (b) the increase of the BAz minor comonomer content.

At lower isothermal crystallization temperatures, the nucleation density was higher than that obtained at higher temperatures, due to the increase in the thermodynamic driving force required for nucleation as supercooling increases [25]. For example, in the case of PBS homopolymer, when the sample is measured at 90 °C, it only takes 3 min to fill the whole microscope field with spherulites. However, when it is measured at 102 °C, more than 1 h is needed for the entire field to be completely filled with crystalline superstructures. This is the expected result, as nucleation tends to be more sporadic as temperature increases.

On the other hand, the incorporation of BAz comonomer significantly increases the nucleation density for the PBS-rich phase. This can be easily appreciated in Fig. 1c, where nucleation density increases with the BAz content, and also in PLOM micrographs of PBSAz copolymers presented in Fig. 2. These micrographs were taken, after the samples were cooled from the melt at 5 °C/min and had impinged on one another, completely filling the microscope observation field (therefore, the temperature at which the images were taken varies depending on the crystallization range of the sample).

The spherulites are negative in all cases, with Maltese Cross extinction patterns. Additionally, regular banding was observed in the PBS-rich copolymer spherulites but not in neat PBS, where some highly irregular banding can only be observed near the spherulite edges in Fig. 2. The addition of miscible "impurities", such as plasticizers and miscible polymeric components is known to induce banding [26]. In the present case, the addition of comonomeric units in a random fashion within the PBS chain also causes a similar effect. The accumulation of the excluded comonomeric units near the lamellar surfaces (it has to be remembered that in these isodimorphic copolymers there are both included and excluded comonomer units within the crystals according to our own previous works) [4,21,22] may be the determining factor to induce banding in the present case.

In the case of the compositions rich in PBAz, although the density of nuclei could not be measured for both samples, the BS$_{25}$BAz$_{75}$ copolymer and PBAz homopolymer, results showed that the incorporation of BS comonomer results in lower nucleation density, the opposite effect of what occurs in the PBS-rich samples. Fig. 3 shows polarized light optical micrographs of both samples after cooling from the melt at 5 °C/min (Fig. 3a–b) and also isothermally crystallized at same supercooling (Fig. 3c–d). The supercooling was calculated with the equilibrium melting temperature (T^0_m) determined here, by using the Thomson-Gibbs method (see the different T^0_m determinations below). When both compositions are cooled from the melt, much lower nucleation density is appreciated in BS$_{25}$BAz$_{75}$ copolymer because the addition of BS comonomer causes an unexpected antinucleation effect. This effect is better appreciated when both are isothermally crystallized at same supercooling (Fig. 3d), where a reduced number of larger spherulites can be appreciated for the copolymer as compared to the PBAz homopolymer.

We speculate that the reason behind the changes in nucleation density with composition is due to the comonomer inclusion within each
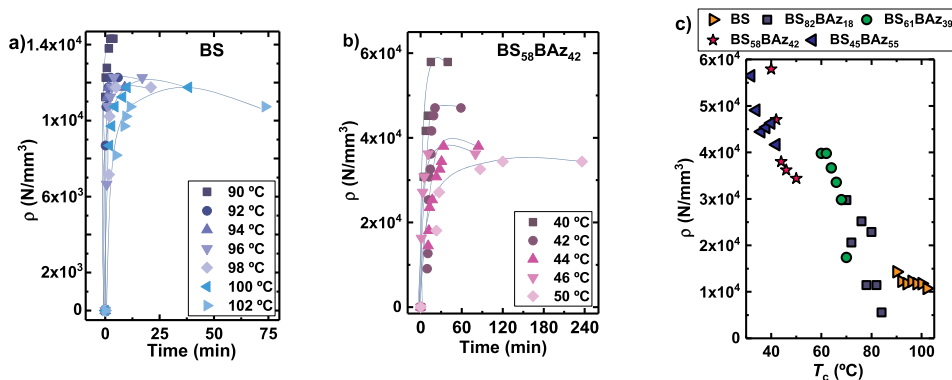
Fig. 1. (a) and (b) Nucleation density as a function of time for PBS and BS$_{58}$BAz$_{42}$ copolymer. (c) Nucleation density at saturation values as a function of crystallization temperature (T_c).
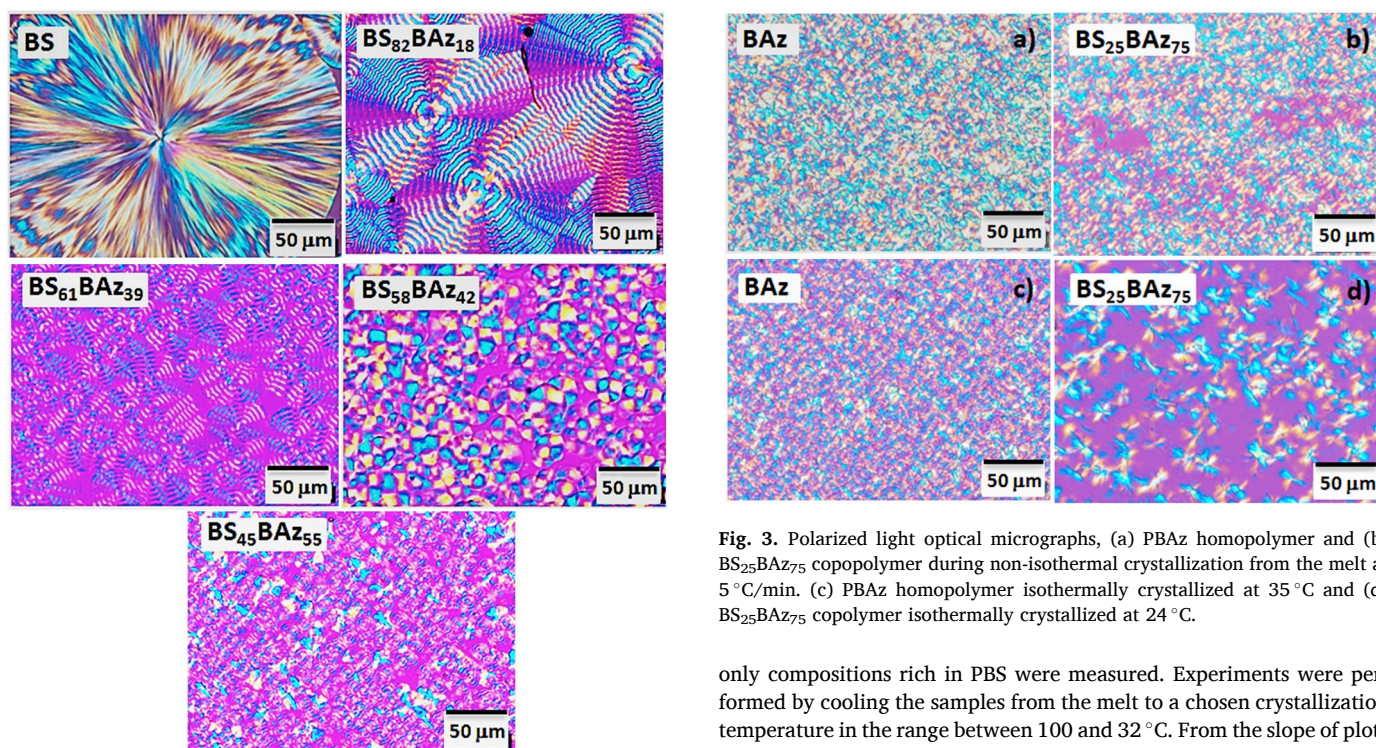

Fig. 2. Polarized light optical micrographs of PBS-rich copolymers during non-isothermal crystallization from the melt at 5 °C/min. Micrographs were taken when spherulites completely covered the microscope field under observation.

Fig. 3. Polarized light optical micrographs, (a) PBAz homopolymer and (b) BS$_{25}$BAz$_{75}$ copolymer during non-isothermal crystallization from the melt at 5 °C/min. (c) PBAz homopolymer isothermally crystallized at 35 °C and (d) BS$_{25}$BAz$_{75}$ copolymer isothermally crystallized at 24 °C.

crystallizing phase. As will be explained below (in Fig. 13), a large amount of PBS comonomer units (up to 20% or more depending on composition) can be included in the PBAz-rich crystals formed, apparently causing some small hindering of the nucleation process. On the other hand, there is a very small incorporation of PBAz (between 1 and 2% maximum, depending on composition) in the PBS-rich crystals apparently favoring the nucleation of this phase. This may be due to a balance between inclusion and exclusion, which can affect the heterogeneous nucleation process, although the exact mechanism is still unknown.

3.2. Kinetics of superstructural growth (secondary nucleation) by PLOM

The spherulitic growth rate of PBS and PBS-rich copolymers as a function of the isothermal crystallization temperature is shown in Fig. 4. As explained before, due to the high nucleation density of some samples,

only compositions rich in PBS were measured. Experiments were performed by cooling the samples from the melt to a chosen crystallization temperature in the range between 100 and 32 °C. From the slope of plots of radius versus time (which were always linear), spherulitic growth rates, G (μm/min), for each composition was determined at different crystallization temperatures.

Fig. 4 shows the spherulitic growth rate G (μm/min) as a function of T_c. In this case, only the right side of the typical bell-shape trend caused by the competition between thermodynamic control of secondary nucleation and diffusion is observed [27]. When lower T_c values were attempted, both the nucleation and growth rates were too high and measurements of spherulitic growth before impingement proved impossible.

The spherulitic growth rate G (μm/min) depends strongly on the copolymer composition, as G dramatically decreases with the increase of BAz-units content. In fact, in comparison with neat PBS, copolymers with 61% PBAz or more can have values of growth rate as low as one order of magnitude lower. As a result, large differences are observed between compositions with only 18% of BAz and compositions with more than 61% of BAz (see Fig. 4a and c).

The supercooling required for crystallization also increases with BAz content in the copolymers, as a result of the change in equilibrium melting temperature with composition. When G is plotted as a function of supercooling ($\Delta T = T_m^0 - T_c$), using the equilibrium melting
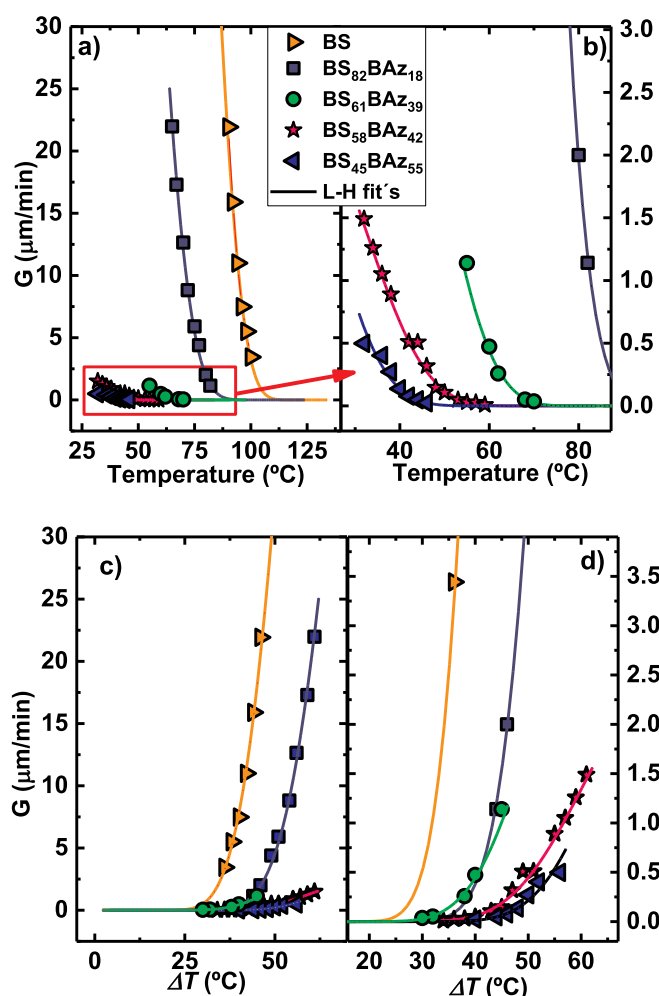
Fig. 4. (a) and (b) spherulitic growth rates determined by PLOM for neat PBS and PBS-rich copolymers. The solid lines are the fits to the Lauritzen−Hoffman (LH) theory. (c) and (d) spherulitic growth rates as a function of supercooling. Note that Fig. 4b and d, correspond to a close-up, so that data for the following samples is better appreciated: BS$_{61}$Baz$_{39}$, BS$_{58}$BAz$_{42}$, BS$_{45}$Baz$_{55}$.

temperatures (T_m^0) determined by the Thomson-Gibbs method (see below), in Fig. 4c and d, the curves are now shifted along the x-axis reducing the differences between the overall crystallization curves versus T_c. Nevertheless, the curves are not completely superimposed, neither on the x-axis nor on the vertical y-axis. This means that the overall crystallization kinetic differences between PBS-rich copolymer chains cannot be normalized by just a single thermodynamic variable (i. e., T_m^0). These results indicate that apart from this thermodynamic effect (i.e., the supercooling), also kinetic effects are influencing chain diffusion of copolymers, as PBS linear sequences are frequently interrupted by BAz repeating units [4].

Summarizing the results obtained so far, the incorporation of BAz units in the random copolymers with a majority of PBS content causes two opposing trends: an increase in nucleation density and a large decrease in spherulitic growth kinetics. The competition between these two factors will determine the overall crystallization rate (that was measured by DSC and will be presented in the next section).

3.3. Overall isothermal crystallization

To determine the overall crystallization rate of PBS, PBAz and PBSAz copolymers, isothermal crystallization experiments were performed by DSC. From DSC experiments, the inverse of the half-crystallization time

($1/\tau_{50\%}$) was determined and plotted against the crystallization temperature (Fig. 5a). The $1/\tau_{50\%}$ value is the inverse of the time needed to achieve the 50% of the total transformation to the semi-crystalline state during the isothermal crystallization process, and with this an experimental measure of the overall crystallization rate, which includes both growth and nucleation contributions, can be quantified.

For those compositions rich in PBS, results show that when the BAz comonomer content increases the inverse of the half-crystallization time decreases, as well as it occurs with the spherulitic growth rate (G), explained above in the text. However, as in the overall crystallization, both nucleation and spherulitic growth rate contribute, in this case, $1/\tau_{50\%}$ does not decrease as dramatically as G with the increase of BAz-units in the copolymer. Therefore, the changes in nucleation density strongly affect the overall crystallization rates determined by DSC, as they compensate the dramatic decrease in G values with comonomer content by increasing the nucleation rate.

On the other hand, it was not possible to measure the nucleation density of both PBAz homopolymer and BS$_{25}$BAz$_{75}$ by PLOM, as they were too high. However, the half-crystallization time ($1/\tau_{50\%}$), determined by DSC for both samples, showed similar behavior as a function of T_c. When these results are plotted against supercooling (ΔT) (Fig. 5b), there are no differences between neat PBAz and the copolymer, and the curves in the x-axis are shifted normalizing the differences in crystallization temperature exhibited by both compositions. Furthermore, the curves are also superimposed on the vertical axis. Although the micrographs in Fig. 3 showed that the density of nuclei decreases when 25% of BS content was added to the copolymer (BS$_{25}$BAz$_{75}$), the overall crystallization rate is not affected, indicating that two important factors may be influencing the crystallization of PBAz-rich copolymers: (a) the addition of BS comonomer has a plasticizing effect in the PBAz-rich phase, and/or (b) the inclusion of BS-units within the PBAz crystallites is significant and the excluded units do not significantly limit crystallization. This latter behavior would be in good agreement with predictions of the Wendling-Suter model (Fig. 13a), as explained below in the text. The results of fitting the T_m^0 data as a function of composition with the Wendling-Suter model indicate that the energy barrier needed in order to introduce BS comonomer units within the PBAz-rich crystalline face is much lower than in the opposite case. In addition, the estimation of the minor comonomer percentage incorporated within PBAz crystals is predicted to be a large relative number.

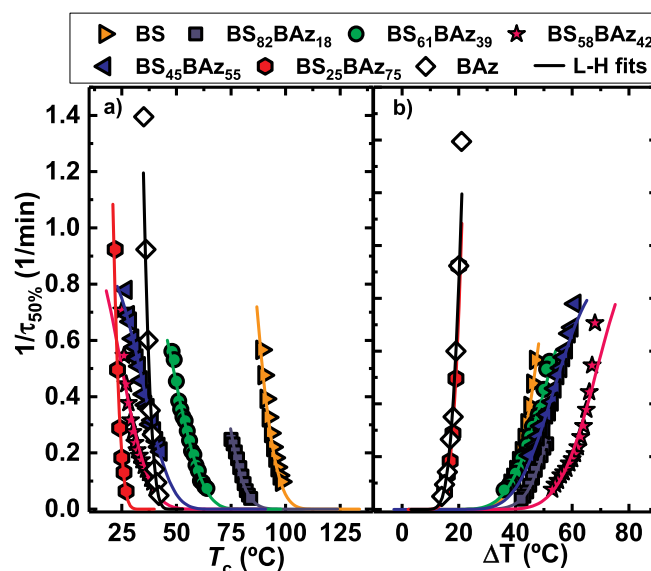In the case of PBS-rich copolymers, Fig. 5b shows that even though

Fig. 5. Inverse of half-crystallization time as a function of (a) T_c and (b) supercooling ΔT for indicated PBSAz samples.

the crystallization curves are brought together when represented as a function of supercooling, there is no perfect superposition between PBS and the PBS-rich copolymers, as in the case of the PBAz-rich copolymer with PBAz. Once again, the thermodynamic parameter (i.e., supercooling) can only partially explain the reduction in crystallization rate caused by PBAz comonomer sequences in the PBS-rich phase. So, kinetic effects, related to both primary and secondary nucleation must be playing a role influenced by the different inclusion/exclusion balance of comonomeric units. In the case of PBS-rich copolymers, we believe that exclusion dominates the behavior. This is consistent with the theoretical predictions of the Wendling-Suter model, to be presented below.

3.4. Fitting of DSC isothermal data to the Avrami model

The isothermal experimental data obtained from the DSC measurements were fitted to the Avrami equation [24,28,29]:

$$1 - V_c(t - t_0) = \exp(-k(t - t_0)^n) \tag{1}$$

where $V_c(t)$ is the relative volumetric transformed fraction as a function of time, t the experimental time and t_0 is the induction time for crystallization. k is the overall crystallization rate constant and n is the Avrami index, which strongly depends on both the time dependence of the nucleation (n_n) and the crystal growth geometry (n_d) [30]. When polymers crystallize with spherulitic-type morphology (3D structure), the Avrami index value is usually in between 3 and 4, whereas when they crystallize with axialites-type morphology (2D aggregates) the Avrami index fluctuates between 2 and 3. But in both cases the final value will always depend on nucleation kinetics. Sporadic nucleation will produce values of $n = 3$ (for axialites) and $n = 4$ (for spherulites. or instantaneous). However, instantaneous nucleation yields n values of 2 and 3 for axialites and spherulites respectively [31,32].

The fits to the Avrami equation were calculated using the free Origin plug-in developed by Lorenzo et al. [24], and in Fig. 6 an example of a representative fit of the Avrami model for the BS$_{25}$BAz$_{75}$ copolymer crystallization at 24 °C is plotted.

Even though Avrami fit estimations were made for all the compositions and at different crystallization temperatures, the result of the BS$_{25}$BAz$_{75}$ copolymer was taken as an example of the good fit between the Avrami model and the experimental data. In Fig. 6c it can be observed how the Avrami equation can perfectly describe the overall crystallization kinetics of the chosen copolymer in the primary crystallization range, i.e., in a conversion range of 3–20%, with a correlation coefficient of 1.000. The fit of the Avrami equation was very good until at least 50% conversion (see Fig. 6a and b) and only experienced significant deviations from the experimental data beyond 75% conversion.

Fig. 7 shows the Avrami index as a function of T_c for all the compositions. Most of the samples exhibited an expected Avrami index value between 2.5 and 4, since by PLOM spherulites were observed for all the samples. In addition, a general trend of increasing the Avrami index with temperature can be observed, due to a more sporadic nucleation produced at lower supercoolings (i.e., high crystallization temperatures). Nevertheless, some compositions exhibited Avrami index values close to 1.5, a value that can be approximated to $n = 2$, corresponding to instantaneously nucleated axialites (or 2D aggregates). If the nucleation density is very high, the development of 3D structures can be limited by their early impingement during growth, thereby forming axialites. The formation of axialites can be due to several reasons. It must be remembered that by adding BAz comonomer units to the PBS-rich copolymers, the nucleation density was greatly enhanced, and the samples in which PBS-rich phase crystallizes but with the highest BAz content show the lowest Avrami index values. On the other hand, the low isothermal temperatures, T_c values, used to study the overall crystallization rate by DSC, can produced an even more instantaneous nucleation. In DSC studies, the overall crystallization kinetics can be determined at lower temperatures than those employed in determining
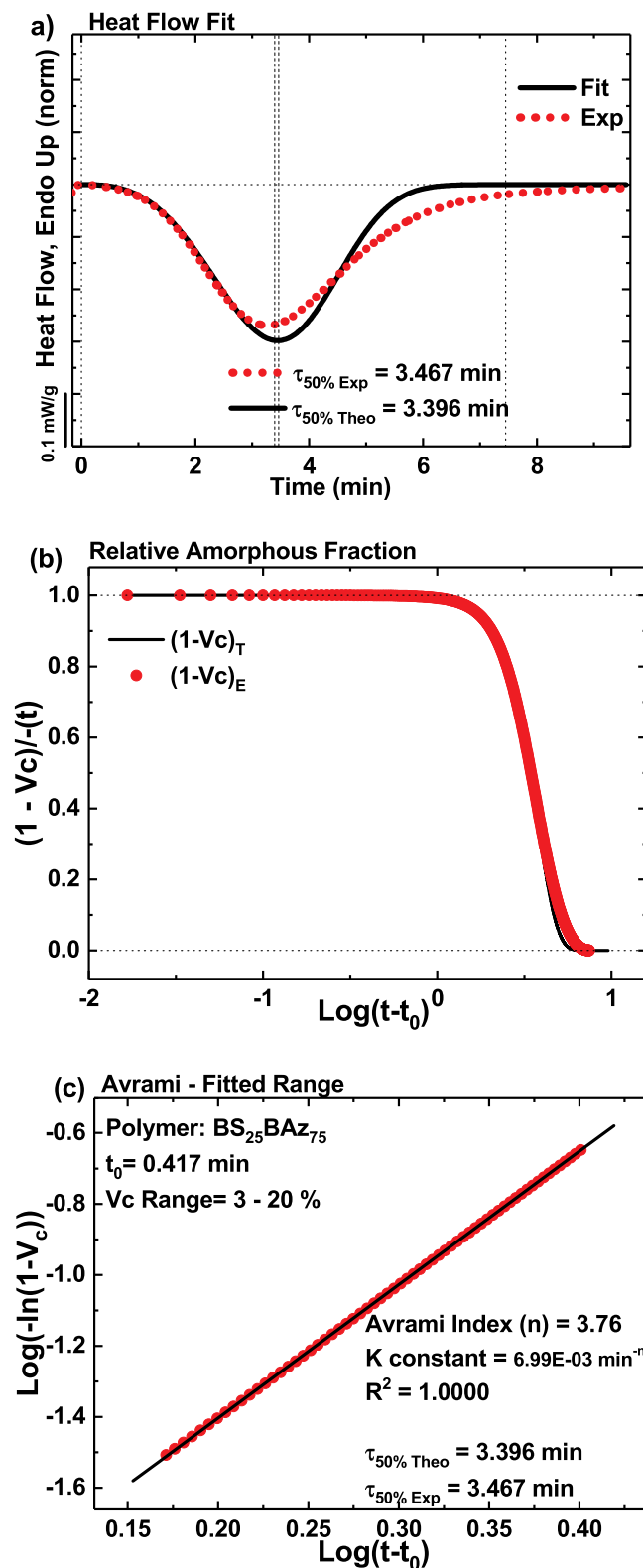

Fig. 6. (a–c) The fits to the Avrami equation using the free Origin plug-in developed by Lorenzo et al. [24] and the experimental data for the BS$_{25}$BAz$_{75}$ copolymer sample.
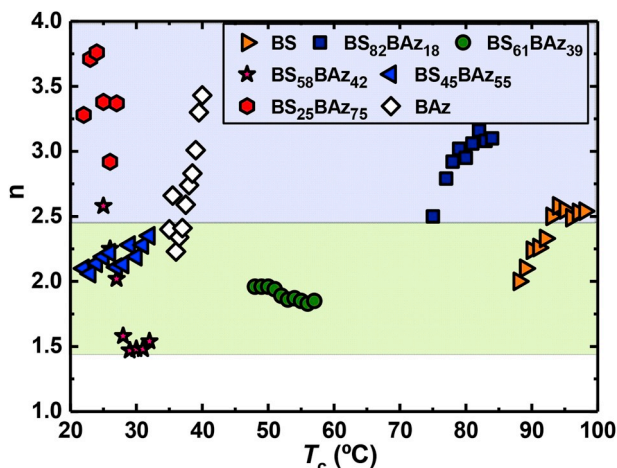
Fig. 7. Avrami index as a function of T_c. The two shaded regions in the plot represent the values corresponding to Avrami indexes that can be approximated to $n = 2$ and those in the upper shaded region, where the Avrami index fluctuates between 2.5 and 3.75, which can be approximated to 3 or 4 respectively.

spherulitic growth kinetics, as long as the sample does not crystallize during the cooling step to T_c (at 60 °C/min).

3.5. Enthalpy of fusion of the 100% crystalline homopolymers

The heat of fusion of a 100% crystalline polymer ($\Delta H^0_{m(100\%)}$) is a required value for the estimation of crystalline fraction of polymers by DSC. In this work, we have reevaluated published values for both PBS and PBAz by employing a combined DSC and X-ray diffraction (WAXS) method.

In order to calculate the $\Delta H^0_{m(100\%)}$ of a polymer, the most commonly used method in the literature is to prepare samples with different crystallinity degrees (applying different cooling rates for instance) and then determine their crystallinities by WAXS. The experimental heats of fusion are determined by DSC, and then a plot is made of WAXS crystallinity degree versus enthalpy of fusion, that is extrapolated to 100% crystallinity. The difficulty in this method is that it is not easy to prepare fast crystallizing polymer samples (like PBS and PBAz) with different crystallinities. In fact, if the available values from the literature are examined [33,34], they were determined by extrapolating 6 or less data points.

In the present work, we propose simple method to determine the 100% enthalpy of fusion of a fast crystallizing polymer by making use of real time WAXS measurements at the synchrotron. A sample of each homopolymer was heated to erase its thermal history (at a temperature 30 °C higher than the melting peak registered by DSC at 10 °C/min) and then cooled at 50 °C/min to a selected crystallization temperature. During the isothermal crystallization process, WAXS patterns were obtained every 10 s until the sample completed its crystallization process. Employing the WAXS patterns, the crystallinity values were calculated using the relative areas under the crystalline peaks. Before the crystallization starts, just when the sample reaches the desired crystallization temperature after cooling from the melt, the sample is in the melt, so the WAXS pattern at time = 0 corresponds to the amorphous halo that is later used for the crystallinity calculations. Fig. 8 shows an example of the WAXS patterns observed at different crystallization times at $T_c = 34$ °C for PBAz homopolymer. The possible temperature differences that may exist between the DSC and the Linkam hot stage were taken into account by comparing the crystallization times that are measured by each technique for the same sample. Then any difference, which in the cases that were detected were always very small (less than 1 °C), can be taken into account by normalization.

In Fig. 9, crystallinity degree values calculated by WAXS are plotted
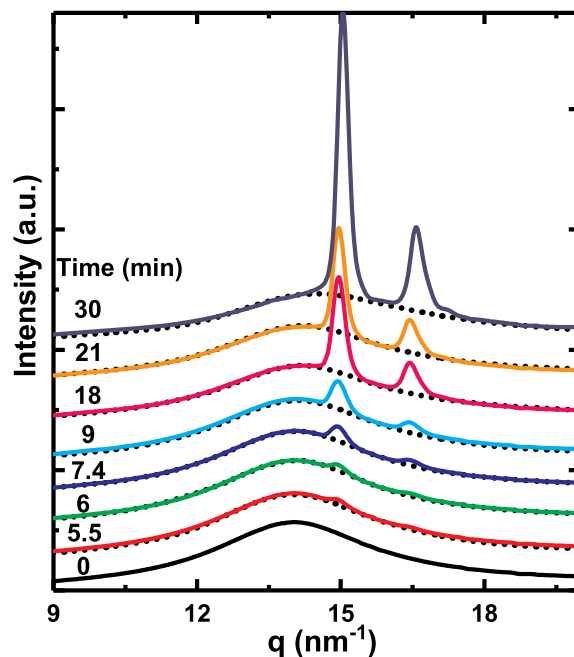

Fig. 8. Selected WAXS patterns for PBAz homopolymer at different crystallization times at 34 °C. The included "dotted line" represents the amorphous halo (i.e., see curve at t = 0 min).
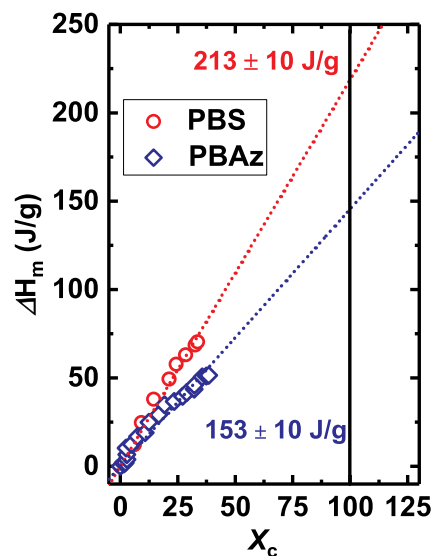

Fig. 9. DSC crystallization enthalpy values as a function of crystallinity degrees obtained by WAXS.

versus the crystallization enthalpy values obtained at each measured time from the respective DSC isothermal curve. Both DSC and WAXS measurements were done at 3 different isothermal temperatures for each homopolymer; however, only one example for PBAz is shown in Fig. 8. The data for the other samples are reported in Figure S2 of the Supplementary Information.

The values obtained with our method for the enthalpy of fusion of the 100% crystalline polyester were found to be $\Delta H^0_{m(100\%)} = 213 \pm 10$ J/g for PBS and $\Delta H^0_{m(100\%)} = 153 \pm 10$ J/g for PBAz. In the case of PBS, this value resulted higher than $\Delta H^0_{m(100\%)} = 110$ J/g estimated empirically by the group contribution method [35], but relatively close to the $\Delta H^0_{m(100\%)} = 210$ J/g reported by Papagerorgiu et al. [34]. In the case of

PBAz, the new value resulted close to the $\Delta H^0_{m(100\%)} = 160$ J/g estimated by the group contribution method [35] and also very close to the $\Delta H^0_{m(100\%)} = 150$ J/g reported by Papagerorgiu et al. [33].

3.6. Equilibrium melting temperature (T^0_m)

The equilibrium melting temperature T^0_m, is the melting point of lamellar crystals of infinite thickness and negligible surface effects on melting. It represents the first order transition of a hypothetical macroscopic perfect crystal [36]. It is very important to determine this parameter in order to analyze the crystallization growth kinetics, and in the case of copolymers every composition will show a different value of T^0_m, as melting is a function of the nature, type and distribution of comonomer units [36]. In this work, several methods have been used to estimate this value.

The first method used to evaluate T^0_m was The Thomson−Gibbs approach [27,37], which is based on the thermodynamic consideration that the melting temperature of a crystal of finite thickness is smaller than that of a crystal of infinite thickness. The Thomson−Gibbs approach is also considered a good way in order to obtain T^0_m values of copolymers, since more than one experimental technique is used for its calculation, such as the DSC and SAXS. The method follows equation (2):

$$T_m = T^\circ_m \left(1 - \frac{2\sigma_e}{l\Delta H_{m\%100}} \right) \qquad (2)$$

where T^0_m is the equilibrium melting temperature, $\Delta H_{m\%100}$ is the enthalpy per unit volume of a perfect crystal (100% crystalline), and σ_e is the fold surface free energy. Following this equation, experimental values of melting temperature obtained by DSC after isothermal crystallization are represented linearly as a function of the inverse of the lamellar thickness (l), determined by SAXS, and the intersection with the ordinate axis will represent the melting temperature of a crystal of infinite thickness, which is the equilibrium melting temperature of the defect-free crystal (Fig. 10b).

For each composition, between 5 and 9 samples were prepared and isothermally crystallized at different temperatures. For that, they were firstly heated to above 30 °C of their melting point during 3 min and afterwards cooled down at 60 °C/min (in order to prevent crystallization during cooling) to a chosen crystallization temperature. The samples were left at those temperatures the time required to crystallize and finally quenched to room temperature. Fig. 10a shows the SAXS measurements performed to BS$_{58}$BAz$_{42}$ samples after the thermal treatment explained above. All samples exhibit a clear intense maximum which is interpreted as the scattering caused by lamellar stacks, and from those q_{max} values, the long periods (d^*) were calculated by equation (3) from Lorentz corrected plots ($I \cdot q^2$ versus q):

$$d^* = (2\pi) / q_{max} \qquad (3)$$

Lamellar thickness (l) values were calculated by employing the approximation $l = x_c \cdot d^*$, where x_c is the crystalline fraction. For that, after the SAXS measurements, DSC heating scans were also performed to the same samples in order to obtain the experimental melting points, melting enthalpies and therefore crystalline fractions [4]. Then applying the Thomson−Gibbs equation [27,37], the inverse of lamellar thickness values were plotted versus the experimental melting points of the isothermally crystallized samples (Fig. 10b), and from the intercept the equilibrium melting temperatures (T^0_m) were determined (see Table 2).

The second method used to estimate T^0_m values was the Hoffman-Weeks plot [38], which involves the extrapolation of a linear region of melting temperatures (T_m) observed experimentally at various crystallization temperatures (T_c), to the thermodynamic equilibrium line $T_m = T_c$ [39,40]. From the intercept T^0_m is calculated.

Fig. 11a shows an example of the DSC heating scans after the previous isothermal crystallization at different temperatures for BS$_{82}$BAz$_{18}$ copolymer. Despite the fact that two peaks were observed at low temperatures, only the peak which varies when the T_c increases was taken into account, since the second peak occurs after a recrystallization process during the heating scan and did not reflect the melting of the isothermally formed crystals. In addition, the extrapolation of melting temperatures T_m to the thermodynamic equilibrium line $T_m = T_c$ of all compositions is observed in Fig. 11b, and T^0_m values of the intercept showed in Table 2.

Table 2 and Fig. 12 report the T^0_m obtained by both methods. For comparison purposes, we include in both Table 2 and Fig. 12 the end melting temperatures determined by DSC on non-isothermally crystallized samples (previously cooled from the melt at 20 °C/min and then heated at the same rate). These are the temperatures where the endothermic signal of the DSC trace finally disappears and joins the DSC base line, i.e., when all traces of crystallinity disappear. These values represent the experimental melting points of the thickest possible lamellae in the material, even if they had reorganized during the heating DSC scans.

Table 2 and Fig. 12 also show the end melting temperatures determined during the final heating DSC scans of samples submitted to Successive Self-nucleation and Annealing (SSA) thermal fractionation obtained from a previous work [21]. The final melting temperature after SSA treatment [41] represents the melting of even thicker lamellae as this method promotes successive annealing.

Hoffman-Weeks and Gibbs-Thomson methods give extrapolated values that theoretically represent the fusion of infinite crystals, without
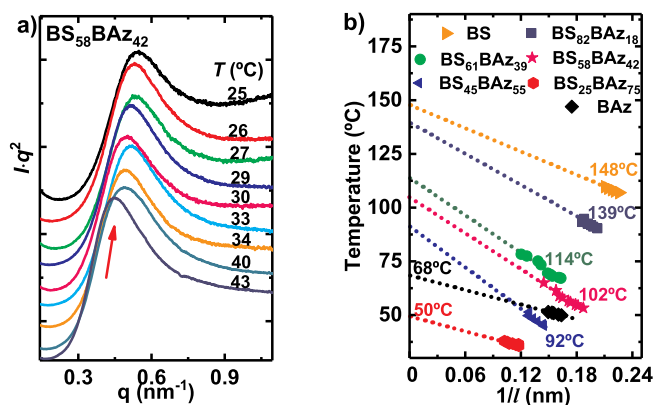

Fig. 10. (a) Lorentz-corrected SAXS profiles, with $I \cdot q^2$ as a function of the scattering vector. (b) Representation of the Thomson−Gibbs plots to obtain $T_m°$ for all PBSAz samples.
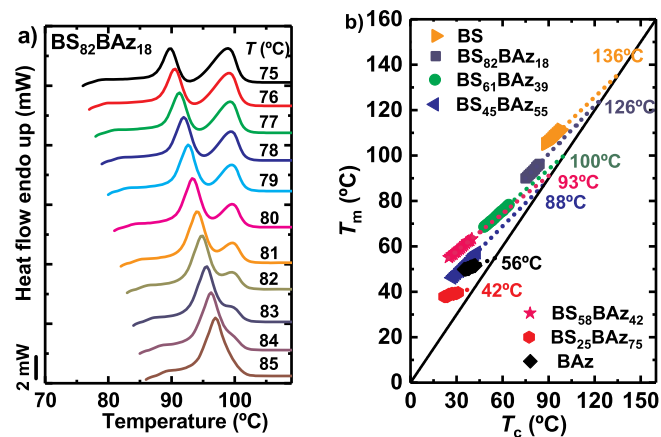

Fig. 11. (a) DSC heating scans after a previous isothermal crystallization at different temperatures in BS$_{82}$BAz$_{18}$ copolymer. (b) Hoffman–Weeks plots for all compositions (the black solid line represents the thermodynamic equilibrium line $T_m = T_c$).

Table 2

Experimentally obtained end melting temperatures ($T_{m(end)}$) and equilibrium melting temperatures, T_m^0 (°C), obtained by different techniques.

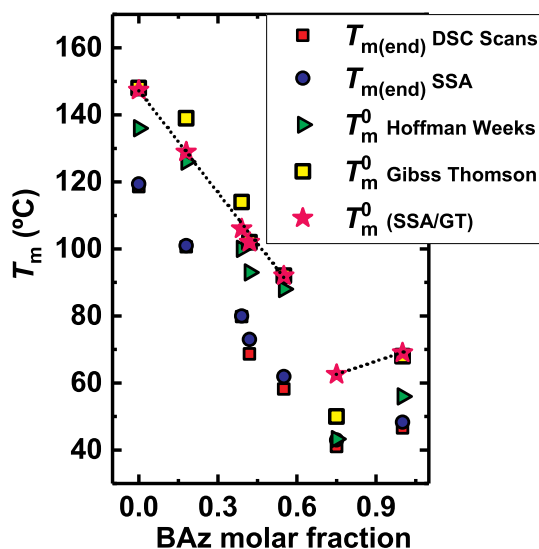|	$T_{m(end)}$ from DSC scans	$T_{m(end)}$ from SSA	T_m^0 Hoffman-Weeks (HW)	T_m^0 Gibbs-Thomson (GT)	$T_{m(SSA/GT)}^0$
BS	118	119	136	148	148
BS$_{82}$BAz$_{18}$	100	101	126	139	129
BS$_{61}$Baz$_{39}$	79	80	100	114	108
BS$_{58}$BAz$_{42}$	68	73	93	102	101
BS$_{45}$BAz$_{55}$	58	62	88	92	90
BS$_{25}$BAz$_{75}$	41	43	42	50	63
BAz	46	48	56	68	68

Fig. 12. Experimentally obtained end melting temperatures ($T_{m(end)}$) and equilibrium melting temperatures, T_m^0 (°C), versus BAz molar content.

surfaces or defects and with extended chains. Therefore, they should always be greater than any experimental value. In general terms, this expectation is corroborated in Table 2 and Fig. 12.

The T_m^0 determined by Hoffman-Weeks for pure PBS (136 °C) is similar to previously reported values (125–134 °C) [34,42–44], and the T_m^0 measured by Gibbs-Thomson (148 °C) is also similar to reported values in the literature that have employed the same method (146.5 °C) [34,43]. In the case of PBAz, only values obtained from Hoffman-Weeks extrapolation were found in literature [23,33], 53 °C and 67 °C respectively which agree very well with the value obtained in this work (56 °C).

In the case of the extrapolated T_m^0 values for the copolymers, determined by both GT and HW methods, a significant scattering of the data as a function of composition can be seen in Fig. 12, which is a consequence of both experimental errors and extrapolation errors.

In order to get a smoother trend with composition, we have performed a reasonable approximation, which is also reported in Table 2 and Fig. 12. In the case of homopolymers, the T_m^0 data is usually considered more reliable than in the case of copolymers [36]. If the data related to PBS in Table 2 is examined, the differences between SSA experimental melting point and the highest T_m^0 values obtained by GT is 29 °C. In other words, the ideal crystals have an equilibrium melting temperature which is 29 °C higher than the apparent or experimentally determined melting temperature of the thickest possible crystals that can be prepared by SSA. Therefore, we have assumed that the 29 °C difference can also hold for the PBS-rich copolymers phase and we have added this constant value to the experimentally determined SSA value in order to estimate T_m^0 values (and they are labeled $T_{m(SSA/GT)}^0$ in Fig. 12)
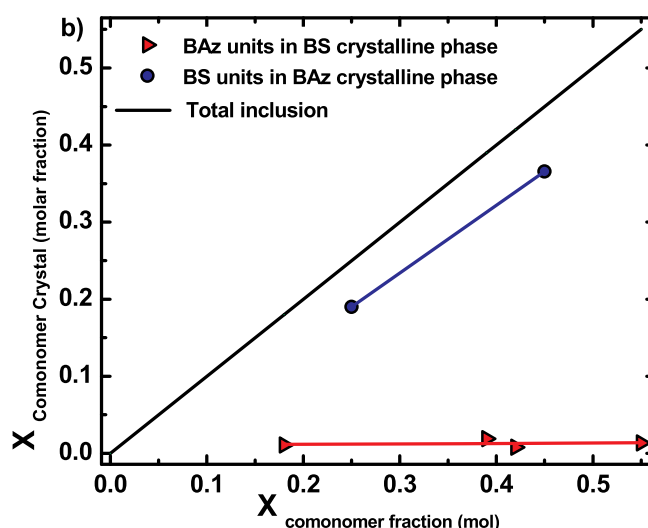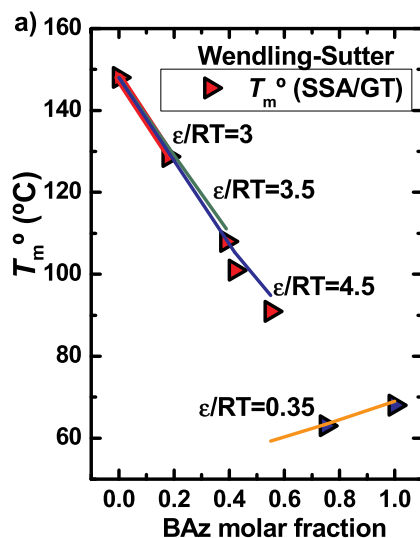

Fig. 13. (a) Comparison of the experimental equilibrium melting temperatures with the theoretical melting temperatures predicted by the Wendling-Sutter equation. (b) Equilibrium concentrations of the minor comonomer units in the crystal of the homopolymer corresponding to the major comonomer, as a function of copolymer composition.

that have a smoother trend with copolymer composition and are in fact not far from the values determined by GT method as reported in Table 2. For PBAz-rich phases, the added factor was 20 °C in correspondence with the difference between SSA experimental melting point and the highest T_m^0 values obtained by GT. Fig. 12 shows straight lines fit for the values corresponding to $T_{m(SSA/GT)}^0$ and it is observed that they can be used as an approximate representation of the variation of T_m^0 with composition, as these values are quite close to those obtained by both GT and HW methods. These $T_{m(SSA/GT)}^0$ values are reported in Table 2 and they were employed to perform the fittings to the copolymer melting theories presented in what follows.

Using the calculated equilibrium melting temperature and following exclusion-inclusion theories, the partitioning of comonomer units between the crystalline and amorphous phase can be analyzed in random copolymers. Those models interpret the effect of exclusion and inclusion of comonomeric sequences in copolymer crystals, or the effect of composition on competition for cocrystallization when inclusion occurs.

The theories that assume comonomer exclusion from the crystal into the amorphous phase are the Flory [45] and Baur [46] exclusion theories. Subsequent theoretical works, Sanchez and Eby [47] or Wendling

and Suter models [48], take into account the inclusion of the comonomer B in crystals of the A repeating unit, suggesting that when the B comonomer is partially included into the crystals of A, it acts as a defect modifying the equilibrium melting point. In order to deal with comonomer inclusions, the defect Gibbs free energy (ε) is included in comonomer inclusion models. Furthermore, Wendling and Suter proposed a more thorough treatment of the problem to account for isodimorphic behavior, employing a new parameter, which considers the comonomer fraction that is cocrystallizing, besides of the above mentioned ε parameter.

The Wendling-Suter model (equation (4)) takes into account the energy required by the minor comonomer repeat units to be introduced into the crystal lattice of the major comonomer and also assumes that the free energy penalty paid to accommodate a defect in the crystal decreases while the amount of included comonomer increases:

$$\frac{1}{T_m^0} - \frac{1}{T_m(X_B)} = \frac{R}{\Delta H_m^0 \left[\frac{\varepsilon X_{CB}}{RT} + (1 - X_{CB}) ln \frac{1 - X_{CB}}{1 - X_B} + X_{CB} ln \frac{X_{CB}}{X_B} + \xi^{-1} \right]} \quad (4)$$

where T_m^0 and ΔH_m^0 are the homopolymer equilibrium melting temperature and heat of fusion, X_B is the concentration of the minor comonomer B in the copolymer, R is the universal gas constant and X_{CB} is the concentration of B units in the crystal. If there is an equilibrium comonomer inclusion, the concentration of comonomer B units in the crystal is given by:

$$X_{CB}^{eq} = \frac{X_B e^{-\varepsilon/RT}}{1 - X_B + X_B e^{-\varepsilon/RT}} \quad (5)$$

and when X_{CB} in equation (4) is substituted by equation (5), it gives a simplified equation:

$$\frac{1}{T_m^0} - \frac{1}{T_m(X_B)} = \frac{R}{\Delta H_m^0} \left\{ ln \left(1 - X_B + X_B e^{-\varepsilon/RT} \right) - \langle \xi \rangle^{-1} \right\} \quad (6)$$

where:

$$\langle \xi \rangle^{-1} = 2 \left(X_B + X_B e^{-\varepsilon/RT} \right) \cdot \left(1 - X_B + X_B e^{-\varepsilon/RT} \right) \quad (7)$$

The ξ parameter takes into account the comonomer units that are cocrystallizing.

In the case of our experimental data we found that the models by Flory, Baur and Sanchez-Eby were not able to give good fits (see Supplementary Information), hence we only present here the fittings performed with the Wendling-Sutter model.

Fig. 13a shows the results of employing the Wendling-Suter model to predict the equilibrium melting temperatures of PBSAz copolyesters (straight lines) in comparison with $T_{m(SSA/GT)}^0$ values previously described (data points).

The results predicted by using Flory, Baur and Sanchez-Eby models are plotted in Figure S3 in the Supporting Information. The Flory and Sanchez-Eby models do not fit the experimental values, since they overestimate the equilibrium melting temperatures. In contrast, the predicted values by the Baur model are the lowest ones, and can partially fit some of the PBS-rich compositions data. However, the Baur model does not fit the PBAz-rich compositions data. The results of applying the Flory, Baur and Sanchez-Eby models are in line with previous works [22], in which it was found that a higher amount of comonomer exclusion dominates over inclusion in isodimorphic copolymers crystallization.

The Wendling-Suter model shows the best fit to the experimental data for lower comonomer content and allows to calculate the defect Gibbs free (ε) energy for each composition. Table 3 shows ε values, calculated from the function ε/RT which was determined as an adjustable parameter. In case of including BAz comonomer units in PBS-rich crystals, ε values tend to increase and they are higher than in the case of incorporating BS repeating units into the PBAz-rich crystal. This ε low

Table 3
Values of the average defect Gibbs energy (ε) and the percentage of comonomer inclusion (X_{CB}) for the PBAz inclusion into a PBS Crystal and for PBS inclusion into BAz Crystals obtained by Fitting Eq. (5) to the experimental data. Note that the subscript indicate which material is included (e.g., $X_{CB, BAz}$ is the percentage of comonomer inclusion of BAz into BS crystals).

PBAz content	$\varepsilon_{CB, BAz}$ (kJ/mol)	$X_{CB, BAz}$
0	0	0
0.18	10.03	0.01081
0.39	11.09	0.01894
0.42	13.99	0.00798
0.55	13.74	0.01339

PBS content	ε_{BS} (kJ/mol)	$X_{CB, BS}$
[a] 0.45	0.68	0.37738
0.25	0.84	0.19803
0	0	0

[a] Value obtained from an extrapolated T_m^0 value.

value indicates that BS units are much easier to include within PBAz crystal unit cells. This result together with Baur's model poor fit, leads to the conclusion that the comonomer inclusion in PBAz-rich phase is larger than expected. Therefore, this theory is in good agreement with the results obtained for the isothermal crystallization of PBAz-rich compositions (Fig. 5b), which showed that when $(1/\tau_{50\%})$ values are plotted against supercooling (ΔT), the curves in the x-axis and vertical axis are superimposed.

The Wendling-Suter model was also used to estimate the percentage of the minor comonomer units incorporated in both cases, for PBS-rich and PBAz-rich crystalline phases. Using Eq. (5), the equilibrium concentration of minor comonomer repeat units into the crystal was calculated (see Table 3) and also plotted as a function of minor comonomer fraction in Fig. 13b.

In the case of PBS-rich compositions, the % comonomer included in the crystal is very small. This is clear in Fig. 13b when the obtained values are compared with total inclusion case ($X_{CB} = X_B$). On the contrary, for PBAz-rich compositions, a large amount of comonomer inclusion is predicted. This latter result is in good agreement with the conclusion obtained in our previous work [22], where dielectric spectroscopy measurements were carried out with same copolymers in order to calculate the relative fractions of both comonomers incorporated in the crystalline phase. In the case of BS$_{25}$BAz$_{75}$ sample, dielectric spectroscopy detected a fraction of BS comonomer units being involved in the crystallization (as it was absent from the amorphous regions). However, DSC indicated for this copolymer that the PBS phase cannot crystallize, therefore it was concluded that these BS units must be incorporated in the PBAz-rich crystalline phase.

4. Conclusions

Two different behaviors were found when analyzing the isothermal crystallization of PBSAz random copolymers. Firstly, the incorporation of BAz-units greatly affected the crystallization of PBS-rich compositions, increasing the density of nuclei and slowing down the spherulitic growth rate due to the difficulty of incorporating units of this minor comonomer inside PBS crystals. On the other hand, a very different behavior was found in PBAz-rich compositions, where the incorporation of BS-units not only did not affect the crystallization of this copolymer significantly, but also caused an antinucleating effect.

The use of the different inclusion-exclusion models together with the calculated equilibrium melting point values allowed us to conclude that in the case of PBS-rich compositions, only a small portion of BAz comonomer units can be included within PBS crystals, while in the case of PBAz-rich compositions, a larger inclusion of BS-units is possible. Results corroborated that the crystallization behavior of isodimorphic copolymers is largely affected by the amount of comonomer inclusion in

their crystal lattices, and consequently it has a direct effect in their crystallinity degree, crystallization rates and in the pseudo-eutectic composition.

Techniques such as WAXS, SAXS and DSC were successfully used in order to calculate the equilibrium melting temperature of these random copolymers. Additionally, the enthalpy of melting of 100% crystalline PBS and PBAz were determined by a different and practical approach: extrapolating real time synchrotron Wide Angle X-ray Scattering (WAXS) isothermal crystallization data and isothermal DSC data.

Acknowledgments

Appendix A. Supplementary data

Supplementary data to this article can be found online at https://doi.org/10.1016/j.polymer.2019.121863.

References

[1] L. Sisti, G. Totaro, P. Marchese, PBS makes its entrance into the family of biobased plastics, in: S. Kalia, L. Averous (Eds.), Biodegradable and Biobased Polymers for Environmental and Biomedical Applications, Scrivener Publishing, Wiley, 2016, pp. 225–285.

[2] P. Pan, Y. Inoue, Polymorphism and isomorphism in biodegradable polyesters, Prog. Polym. Sci. 34 (2009) 605–640.

[3] I. Arandia, A. Mugica, M. Zubitur, A. Arbe, G. Liu, D. Wang, R. Mincheva, P. Dubois, A.J. Müller, How composition determines the properties of isodimorphic poly(butylene succinate-ran-butylene azelate) random biobased copolymers: from single to double crystalline random copolymers, Macromolecules 48 (2015) 43–57.

[4] C. Bastioli, G. Del Tredici, I. Guanella, T. Milizia, R. Ponti, Mixtures of Biodegradable Polyesters and Products Manufactured from Them, Novamont Granted Patent, EP 1947145 B1, 149-150-130-770-562, (2009).

[5] G. Wang, Z. Qiu, Synthesis, Crystallization kinetics, and morphology of novel biodegradable poly(butylene succinate-co-hexamethylene succinate) copolyesters, Ind. Eng. Chem. Res. 51 (2012) 16369–16376.

[6] M. Ren, J. Song, C. Song, H. Zhang, X. Sun, Q. Chen, H. Zhang, Z. Mo, Crystallization kinetics and morphology of poly(butylene succinate-co-adipate), J. Polym. Sci., Part B: Polym. Phys. 43 (2005) 3231–3241.

[7] R.A. Pérez-Camargo, B. Fernández-d'Arlas, D. Cavallo, T. Debuissy, E. Pollet, L. Avérous, A.J. Müller, Tailoring the structure, morphology, and crystallization of isodimorphic poly(butylene succinate-ran-butylene adipate) random copolymers by changing composition and thermal history, Macromolecules 50 (2017) 597–608.

[8] J.B. Zeng, C.L. Huang, L. Jiao, X. Lu, Y.Z. Wang, X.L. Wang, Synthesis and properties of biodegradable poly(butylene succinate-co-diethylene glycol succinate) copolymers, Ind. Eng. Chem. Res. 51 (2012) 12258–12265.

[9] H.M. Ye, R.D. Wang, J. Liu, J. Xu, B.H. Guo, Isomorphism in poly (butylene succinate-co-butylene fumarate) and its application as polymeric nucleating agent for poly (butylene succinate), Macromolecules 45 (2012) 5667–5675.

[10] R.A. Pérez-Camargo, I. Arandia, M. Safari, D. Cavallo, N. Lotti, M. Soccio, A. J. Müller, Crystallization of isodimorphic aliphatic random copolyesters: pseudo-eutectic behavior and double-crystalline materials, Eur. Polym. J. 101 (2018) 233–247.

[11] Y.G. Jeong, W.H. Jo, S.C. Lee, Cocrystallization behavior of poly(butylene terephthalate-co-butylene 2,6-naphthalate) random copolymers, Macromolecules 33 (2000) 9705–9711.

[12] G. Allegra, I.W. Bassi, Isomorphism in synthetic macromolecular systems, Fortschritte der Hochpolymeren-Forschung, Springer Berlin, 1969, pp. 549–574.

[13] Y. Yu, L. Sang, Z. Wei, X. Leng, Y. Li, Unique isodimorphism and isomorphism behaviors of even-odd poly (hexamethylene dicarboxylate) aliphatic copolyesters, Polymer 115 (2017) 106–117.

[14] J.P. Latere Dwan'Isa, P. Lecomte, P. Dubois, R. Jérôme, Synthesis and characterization of random copolyesters of ε-caprolactone and 2-oxepane-1, 5-dione, Macromolecules 36 (2003) 2609–2615.

[15] G. Ceccorulli, M. Scandola, A. Kumar, B. Kalra, R.A. Gross, Cocrystallization of random copolymers of ω-pentadecalactone and ε-caprolactone synthesized by lipase catalysis, Biomacromolecules 6 (2005) 902–907.

[16] L. Sheng, R.A. Register, Crystallization in copolymers, in: E. Piorkowska, G. C. Rutledge (Eds.), Handbook of Polymer Crystallization, Wiley, Hoboken, 2013, pp. 327–346.

[17] R. Mincheva, A. Delangre, J.M. Raquez, R. Narayan, P. Dubois, Biobased polyesters with composition-dependent thermomechanical properties: synthesis and characterization of poly(butylene succinate-co-butylene azelate), Biomacromolecules 14 (2013) 890–899.

[18] T. Fujimaki, Processability and properties of aliphatic polyesters, 'BIONOLLE', synthesized by polycondensation reaction, Polym. Degrad. Stab. 59 (1998) 209–214.

[19] G.Q. Chen, M.K. Patel, Plastics derived from biological sources: present and future: a technical and environmental review, Chem. Rev. 112 (2012) 2082–2099.

[20] J. Xu, B.H. Guo, Microbial succinic acid, its polymer poly(butylene succinate), and applications, in: G.G.Q. Chen (Ed.), Plastics from Bacteria: Natural Functions and Applications, Springer Berlin Heidelberg, 2010, pp. 347–388.

[21] I. Arandia, A. Mugica, M. Zubitur, A. Iturrospe, A. Arbe, G. Liu, R. Mincheva, P. Dubois, A.J. Müller, Application of SSA thermal fractionation and X-ray diffraction to elucidate comonomer inclusion or exclusion from the crystalline phases in poly(butylene succinate-ran-butylene azelate) random copolymers, J. Polym. Sci., Part B: Polym. Phys. 54 (2016) 2346–2358.

[22] I. Arandia, A. Mugica, M. Zubitur, P. Mincheva, P. Dubois, A.J. Müller, A. Alegría, The complex amorphous phase in poly(butylene succinate-ran-butylene azelate) isodimorphic copolyesters, Macromolecules 50 (2017) 1569–1578.

[23] A. Diaz, L. Franco, J. Puiggali, Study on the crystallization of poly(butylene azelate-co-butylene succinate) copolymers, Thermochim. Acta 575 (2014) 45–54.

[24] A. Lorenzo, M. Arnal, J. Albuerne, A. Müller, DSC isothermal polymer crystallization kinetics measurements and the use of the Avrami equation to fit the data: guidelines to avoid common problems, Polym. Test. 26 (2007) 222–231.

[25] R.J. Young, P.A. Lovell, Introduction to Polymers, third ed., CRC Press, Routledge, 2011.

[26] B. Crist, J.M. Schultz, Polymer spherulites: a critical review, Prog. Polym. Sci. 56 (2016) 1–63.

[27] U.W. Gedde, Polymer Physics, Chapman & Hall, London, 1995.

[28] G. Reiter, G.R. Strobl, Progress in Understanding of Polymer Crystallization, Springer, Berlin, 2007.

[29] M. Avrami, Granulation, phase change, and microstructure kinetics of phase change. III, J. Chem. Phys. 9 (1941) 177–184.

[30] A.J. Müller, V. Balsamo, M.L. Arnal, Nucleation and crystallization in diblock and triblock copolymers, Adv. Polym. Sci. 190 (2005) 1–63.

[31] L. Mandelkern, Crystallization of Polymers: Volume 2, Kinetics and Mechanisms, Cambridge University Press, 2004.

[32] J.M. Schultz, Polymer crystallization: the development of crystalline order in thermoplastic polymers, J. Am. Chem. Soc. 124 (2002) 7251–7252.

[33] G.Z. Papageorgiou, D.N. Bikiaris, D.S. Achilias, E. Papastergiadis, A. Docoslis, Crystallization and biodegradation of poly(butylene azelate): comparison with poly (ethylene azelate) and poly(propylene azelate), Thermochim. Acta 515 (2011) 13–23.

[34] G.Z. Papageorgiou, D.N. Bikiaris, Crystallization and melting behavior of three biodegradable poly(alkylene succinates). A comparative study, Polymer 46 (2005) 12081–12092.

[35] D.W. Van Krevelen, K. Te Nijenhuis, D.W. van Krevelen, in: K.T. Nijenhuis (Ed.), Chapter 5, Calorimetric Properties, Properties of Polymers, fourth ed., Elsevier, Amsterdam, 2009, pp. 109–128.

[36] L. Mandelkern, Crystallization of Polymers: Volume 1, Equilibrium Concepts, Cambridge University Press, 2002.

[37] J.D. Hoffman, Theoretical aspects of polymer crystallization with chain folds: bulk polymers, Polym. Eng. Sci. 4 (1964) 315–362.

[38] J.D. Hoffman, J.J. Weeks, Melting process and the equilibrium melting temperature of polychlorotrifluoroethylene, J. Res. Natl. Bur. Stand. Sec. A 66a (1962) 13–28.

[39] J.D. Hoffmann, G.T. Davis, J.I. Lauritzen Jr., The rate of crystallization of linear polymers with chain folding, in: H.B. Hannay (Ed.), Treatise on Solid State Chemistry, Plenum Press, New York, 1976.

[40] J.D. Hoffman, R.L. Miller, Kinetic of crystallization from the melt and chain folding in polyethylene fractions revisited: theory and experiment, Polymer 38 (1997) 3151–3212.

[41] Z.H. Hernandez, A.J. Müller, M.L. Arnal, J.J. Sánchez, Successive self-nucleation/annealing (SSA): a novel technique to study molecular segregation during crystallization, Polym. Bull. 39 (1997) 465–472.

[42] H.M. Ye, Y.R. Tang, J. Xu, B.H. Guo, Role of poly (butylene fumarate) on crystallization behavior of poly(butylene succinate), Ind. Eng. Chem. Res. 52 (2013) 10682–10689.

[43] Z. Gan, H. Abe, H. Kurokawa, Y. Doi, Solid-state microstructures, thermal properties, and crystallization of biodegradable poly (butylene succinate) (PBS) and its copolyesters, Biomacromolecules 2 (2001) 605–613.

[44] Y. Zheng, G. Tian, J. Xue, J. Zhou, H. Huo, L. Li, Effects of isomorphic poly (butylene succinate-co-butylene fumarate) on the nucleation of poly (butylene succinate) and the formation of poly (butylene succinate) ring-banded spherulites, CrystEngComm 20 (2018) 1573–1587.

[45] P.J. Flory, Theory of crystallization in copolymers, Trans. Faraday Soc. 51 (1955) 848–857.

[46] V.H. Baur, Einfluß der sequenzlängenverteilung auf das schmelz-ende von copolymeren, Makromol. Chem. 98 (1966) 297–301.

[47] I. Sanchez, R. Eby, Thermodynamics and crystallization of random copolymers, Macromolecules 8 (1975) 638–641.

[48] J. Wendling, U.W. Suter, A new model describing the cocrystallization behavior of random copolymers, Macromolecules 31 (1998) 2516–2520.